BIOCHEMISTRY
including biophysical chemistry & molecular biology
Article

Biochemistry **2010,** *49,* 3723–3732 3723
DOI: 10.1021/bi100234v

Catalytic Importance of a Protonated Adenosine in the Hairpin Ribozyme Active Site†

Ian T. Suydam, Stephen D. Levandoski, and Scott A. Strobel*

Department of Molecular Biophysics and Biochemistry and Department of Chemistry, Yale University, 260 Whitney Avenue, New Haven, Connecticut 06520-8114

Received February 15, 2010; Revised Manuscript Received April 5, 2010

ABSTRACT: The hairpin ribozyme accelerates the rate of phosphodiester transfer reactions by at least 5 orders of magnitude. To achieve this rate enhancement, the active site forms via a substrate helix docking event that constrains the scissile phosphate linkage and positions G8 and A38 for catalysis, both of which have been implicated as sites of proton transfer in general acid−base catalysis. To investigate the functional groups required for hairpin activity, we previously reported a series of nucleotide analogue interference mapping experiments [Ryder, S. P., et al. (2001) *RNA 7*, 1454−1463]. The critical functional groups implicated in those studies were largely consistent with subsequent X-ray crystal structures, but the lack of A38 interference with 8-azaadenosine (n^8A), a pK_a perturbed nucleotide analogue, argued against functional base ionization at this site. This is inconsistent with a transition state crystal structure and other biochemical studies. To address this discrepancy, we investigated the hairpin ribozyme with an expanded set of pK_a perturbed adenosine analogues containing fluorine. A38 was the only site that showed persistent and strong interference with low pK_a analogues across a variety of construct/substrate pairs. This interference pattern suggests that A38 base ionization is required for catalytic activity. The lack of n^8A interference at A38, in spite of its reduced pK_a, likely results from n^8A stabilization of the docked state, which requires an unusual syn glycosidic base conformation at A38 for active site assembly. The fluorinated adenosine analogues are better suited to identify sites of functional ionization in systems where structural rearrangements are closely coupled to catalytic steps. All pK_a reduced analogues, including those of the previous study, produce selective interference at A38 when substrates are stably bound and docked, consistent with the importance of base ionization at this site.

The hairpin ribozyme is a member of the nucleolytic class of ribozymes, a collection of small protein-independent catalytic RNAs whose members also include the hammerhead, hepatitis delta, Varkud satellite, and glmS ribozymes (*1*). These self-cleaving RNAs catalyze a site-specific and reversible phosphodiester transfer reaction in which the 2′-hydroxyl of an upstream nucleotide attacks the adjacent phosphodiester linkage, producing cleavage products with free 5′-hydroxyl and 2′,3′-cyclic phosphate termini. This concerted S_N2-type reaction requires an in-line geometry of the 2′-hydroxyl, scissile phosphate, and 5′-oxygen leaving group. In the hairpin ribozyme, this scissile phosphate orientation, as well as the positioning of active site residues, is only obtained after a structural transition from an extended (undocked) to condensed (docked) state. The reaction products formed by nucleolytic ribozymes are distinct from those of self-splicing introns and RNase P, and unlike these larger ribozymes, all known members of the nucleolytic class retain catalytic activity in the absence of divalent cations (*1*). This observation in combination with a growing wealth of structural data for several members of the class suggests nucleolytic ribozymes may employ their nucleobases directly in catalysis. The exact nature of nucleobase contribution, either as sites of proton transfer, as the source of electrostatic stabilization, or in the positioning of substrates or bound water molecules, is an unresolved question.

Several factors make the hairpin ribozyme uniquely suited for mechanistic studies. First is the observation that the hairpin readily catalyzes both cleavage and ligation and that the reaction can be driven in either direction by the appropriate choice of construct and cleaved product sequence (*2*). The reversibility of the reaction is essential to the hairpin's function in the replication cycle of the tobacco ringspot virus satellite RNA (*3*) and allows the contribution of particular functional groups for the forward and reverse reactions to be dissected. Another attractive feature of the hairpin is that it can be reassembled from shorter oligonucleotides in a number of combinations, which allows site-specific modifications at nearly any residue. This strategy has been used extensively to prepare constructs for X-ray crystallography with a wide variety of synthetic modifications at the scissile phosphate and at active site residues. To date, nearly 30 hairpin structures have been solved in constructs prepared to mimic the precatalytic, postcleavage, and transition states (*1*). In several of these studies the effect of base modifications on catalysis has also been measured (*4*−*7*). Finally, the ability to introduce fluorophores into active constructs has allowed detailed studies of hairpin dynamics by equilibrium and single-molecule FRET[1] (*8*). These studies have provided some of the most detailed descriptions to date on the connection between RNA dynamics, folding, and catalysis.

Despite the success of site-specific incorporation strategies, their application is constrained by the need to synthesize and

†This work was supported in part by the National Science Foundation (MCB-0544255). I.T.S. acknowledges the NIH for a NRSA postdoctoral fellowship (GM-078764).

*To whom correspondence should be addressed. Phone: (203) 432-9772. Fax: (203) 432-5767. E-mail: scott.strobel@yale.edu.

[1]Abbreviations: NAIM, nucleotide analogue interference mapping; 2WJ, two-way junction; 4WJ, four-way junction; NT, nucleotide; FRET, Förster resonance energy transfer; HDV, hepatitis delta virus.

Published on Web 04/08/2010

reassemble RNAs for each modification and site of interest, which limits the number of sites that can be reasonably investigated. In addition, when truncated constructs are used for site-specific incorporation, they often exhibit significantly perturbed kinetic properties, even when wild-type sequences are used, an effect attributed to the decreased stability of minimal constructs. This problem is especially pronounced for the hairpin ribozyme, where the native sequence includes a four-way helical junction (4WJ) but where the majority of chemical modification experiments have been conducted in a minimal two-way junction (2WJ) construct. Although the active sites of the 2WJ and 4WJ constructs have been shown to be nearly identical by X-ray crystallography (*9*, *10*), the 4WJ folds much faster and more stably (*11*, *12*), favors the ligated state to a greater extent (*2*), exhibits a different pH dependence (*13*−*15*), and functions at physiological salt concentrations where the 2WJ construct is inactive (*16*).

An alternative to site-specific incorporation strategies is nucleotide analogue interference mapping (NAIM). NAIM employs a series of phosphorothioate-tagged triphosphates, each carrying a chemical modification, which are introduced randomly into an RNA by transcription. Transcriptions are carried out such that any individual transcript includes at most one substitution at a random location. This pool of analogue-substituted RNAs is then subjected to a competitive selection, and the active fraction is cleaved at the phosphorothioate tag. Gel electrophoresis of the cleaved RNAs reveals sites of analogue interference (for reviews of the NAIM technique, see refs (*17*−*19*)). There are two main advantages that NAIM has over site-specific substitutions. NAIM can rapidly assay the effect of a chemical modification at all positions simultaneously but on a site by site basis, and the technique can be applied to any RNA sequence that can be transcribed and has a selectable function.

In two early studies of hairpin catalysis a NAIM study of the hairpin ligation reaction used 17 nucleotide analogues to study a 2WJ construct and three analogues to study a 4WJ construct (*20*, *21*). The resulting interference pattern was highly consistent with contacts observed in the subsequent crystal structure of a precleavage 4WJ construct (*22*). The close agreement also helped to establish that two earlier NMR structures of isolated loops A and B were in inactive undocked conformations (*23*−*25*). Despite an overall high level of correspondence, the interference pattern produced by 8-azaadenosine (n^8A) at three active site residues, A9, A10, and A38, did not match the X-ray structure (*25*). This analogue has an N1 pK_a value of 2.2, more than a full pK_a unit below that of A (N1 pK_a = 3.5), and was used to identify sites of adenosine base ionization that are important for function (*21*). In the context of a 2WJ construct n^8A produced strong interference at A10, which could be rescued at low pH, showed enhancement at A9, and had no effect at A38. These data suggested adenosine ionization was required at A10, with this base acting either as a site of proton transfer or as the origin of electrostatic stabilization. Although this pattern of interference did not obviously match the precleavage crystal structure, where the N1 nitrogen of A10 is at least 7 Å from any atoms in the scissile linkage, it was suggested that a modest structural rearrangement in the postcleavage or transition state would be sufficient to bring A10 into hydrogen-bonding distance with the nucleophile, leaving group, or scissile phosphate oxygens (*25*). A rearrangement of this type would also be required to explain the lack of interference at A38, which is much closer to each of these functionalities in the precleavage structure (*22*).

Several lines of evidence now argue against this interpretation of the n^8A interference data and have motivated the current study. Since the initial report of the precleavage 4WJ structure, two additional structures have been reported using the same construct, one with a pentacoordinated vanadate at the location of the scissile phosphate as a transition state mimic and one representing the postcleavage (preligation) state (*9*). All three structures show very similar active site geometries, suggesting a relatively rigid active site throughout the reaction and argue against a structural rearrangement sufficient to bring A10 into direct contact with either the nucleophile or leaving group (*26*). A large collection of crystal structures solved with 2WJ constructs also exhibit the same general active site geometry(*1*). In addition, two structures prepared to mimic the transition state show very short distances between the N1 of A38 and the 5′-oxygen at the cleavage site, consistent with a protonated adenosine at A38 (*9*, *10*). A number of kinetic studies have also investigated the relative importance of active site adenosines and have consistently pointed toward A38 rather than A10 as a site of functional ionization (*27*, *28*). It has also been argued that a lack of interference at A38 from n^8A substitution is not necessarily inconsistent with A38 acting as a general base for ligation reaction, given this analogue's relatively modest pK_a perturbation (*29*). Perhaps most convincing is a recent series of structural and kinetic studies with N1-deazaadenosine incorporated site-specifically at A10 and A38 that clearly demonstrated an essential role for the N1 nitrogen of A38 but not A10 (*4*, *5*). Recent pH-dependent Raman studies also indicate that the pK_a of A38 is shifted toward neutrality in the folded ribozyme, further supporting its potential role as a site of proton transfer (*30*). Taken together, these results argue strongly for functional ionization at A38, not A10, and have inspired us to return to the hairpin ligation reaction using NAIM with additional analogues and constructs.

We recently developed a series of fluorine-substituted adenosine analogues that produce very large changes in N1 pK_a values without significant structural perturbation to the nucleobase (*31*). These include 7-fluoro-7-deazaadenosine (7F-7dA), 2-fluoro-7-deazaadenosine (2F-7dA), and 2-fluoroadenosine (2F-A). The application of these analogues in a NAIM study of the Varkud satellite ribozyme resulted in a very selective interference pattern, showing interference at only 3 of the 36 resolvable adenosine sites. Of these sites, a single adenosine, A756, exhibited an interference pattern consistent with functional ionization (*31*). Significantly, this site was previously shown to exhibit a pH-dependent interference pattern with n^8A (*32*) and has also been implicated as a site of proton transfer by a number of site-specific chemical modification experiments (*33*−*35*). In this study we have applied these fluorine-substituted adenosine analogues to the hairpin ribozyme in an effort to clarify the dependence of interference values relative to the analogue's N1 pK_a value (Figure 1).

Since our initial NAIM studies a great deal has been learned regarding the influence of construct design, substrate binding affinity, and reaction conditions on observed hairpin kinetics (*1*, *8*, *36*). Of greatest significance to the interpretation of NAIM data is the observation that the ligation/cleavage reaction reaches rapid equilibrium in many constructs and that release of initially ligated substrate can also be rapid depending on the stability of the docked state. To explore the effect of construct/substrate identity on observed interference values, we chose four construct/substrate pairings studied extensively by Fedor and colleagues

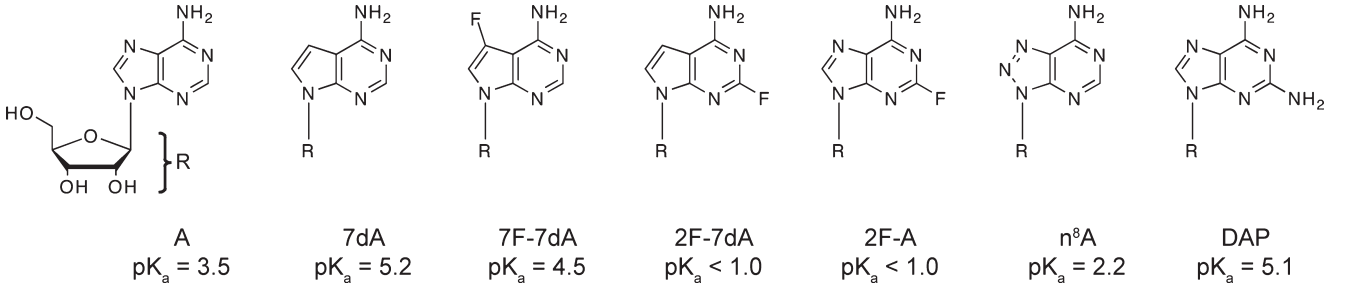

FIGURE 1: Structures and N1 pK_a values of adenosine analogues used in this study (*21*, *31*, *40*).

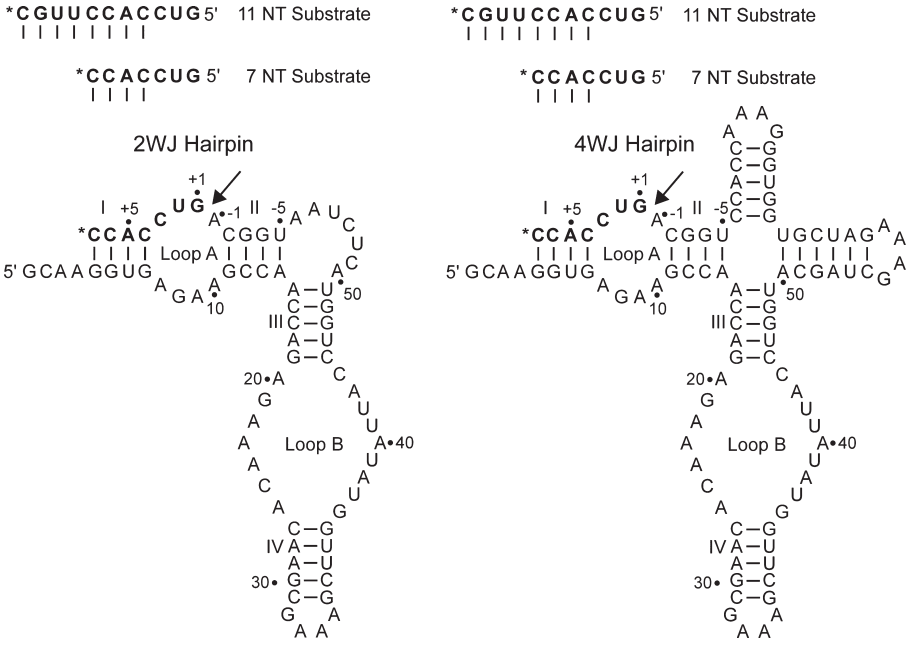

FIGURE 2: Hairpin constructs used in this study containing minimal two-way or native four-way junctions (site of ligation indicated with an arrow). The 3′-end-labeled substrates used for selections (7NT and 11NT) are also shown and are designed to form four or eight base pairs in stem I.

(*2*, *27*) (Figure 2) and conducted NAIM selections in reaction conditions that reflect those used in the majority of kinetic experiments. These NAIM selections reveal that many of the observed interferences are highly dependent on substrate binding affinity and the stability of the docked state. For constructs with stably bound and docked substrates, the observed interference pattern is highly selective and consistent with an essential role for A38 ionization in catalysis.

EXPERIMENTAL PROCEDURES

Plasmid Templates for Hairpin Ribozyme Transcriptions. 2WJ and 4WJ hairpin sequences were amplified from overlapping DNA primers and cloned into pUC19 following standard procedures. An antigenomic HDV ribozyme sequence was introduced at the 3′-end of each hairpin sequence to produce the desired 2′,3′-cyclic phosphate terminus. Following the HDV sequence an *Ssp*I restriction site was introduced to produce a blunt-end linearized DNA template. For the 2WJ construct the linearized template had the following sequence (promoter in bold, hairpin sequence underlined, HDV sequence uppercase, *Ssp*I site lowercase): **TAATACGACTCACTATA**GCAAGGTGAGAAGCCAACCAGAGAAACACAAGCGAAAGCTTGGTATATTACCTGGTACTCTAATGGCAGGGTCGGCATGGCATCTCCACCTCCTCGCGGTCCGACCTGGGCATCCGAAGGAGGACAGACGTCCACTCGGATGGCTAAGGGAGAGCCAaat. For the 4WJ construct the hairpin sequence was replaced with the following: GCAAGGTGAGAAGCCAACCAGAGAAACACAAGCGAAAGCTTGGTATATTACCTGGTACGATCGAAAGATCGTGGTGGGAAACCACCTGGCA. Sequenced plasmids were completely digested with *Ssp*I to form linear templates. Typical digestions contained 100 ng/μL plasmid and 2 units/μg *Ssp*I and were incubated at 37 °C for 2 h. The restriction enzyme was denatured at 65 °C for 20 min, and the templates were used in transcriptions without further purification.

Ligation Substrates. Ligation substrates were synthesized and deprotected according to the manufacturer's protocol (Dharmacon). Two substrates, denoted 7NT and 11NT, were used for NAIM experiments (7NT, GUCCACC; 11NT, GUCCACCUUGC). Each substrate was labeled at the 3′-end with 1 equiv of [α-^{32}P]pCp by T4 RNA ligase, purified by 20% nondenaturing PAGE, and eluted into $T_{10}E_{0.1}$ overnight at 4 °C. After the addition of pCp, the 7NT substrate forms four base pairs in helix I, with a 3′ A·C mismatch, while the 11NT substrate forms eight base pairs with a 3′ C overhang.

Hairpin Transcription. Unligated 2WJ and 4WJ hairpin RNA was obtained by transcription of *Ssp*I linearized plasmids. Typical 100 μL transcriptions contained 40 mM Tris buffer (pH = 8.0), 15 mM $MgCl_2$, 2 mM spermidine, 5 mM DTT, 0.005% Triton X-100, 1 mM each NTP, 2 μg of *Ssp*I cut plasmid,

1 unit of inorganic pyrophosphatase (Sigma), and T7 RNA polymerase to a final concentration of 0.1 mg/mL. Hairpin RNAs with randomly incorporated nucleotide analogues were obtained by including the corresponding 5′-*O*-(1-thio)nucleoside triphosphates to final concentrations described previously (*17*). Transcriptions were incubated for 2.5 h at 37 °C, then heated to 70 °C, and slow cooled to 25 °C over 45 min. This refolding step led to complete cleavage of the inserted HDV ribozyme, producing unligated hairpin RNAs with the desired 2′,3′-cyclic phosphate at the A(−1) position. RNAs were purified by 8% denaturing PAGE and eluted at 25 °C for 1 h into $T_{10}E_{0.1}$, 250 mM NaCl, and 2% (w/w) SDS. Elutions were PCA extracted (phenol/chloroform/isoamyl alcohol (25:24:1) saturated with 10 mM Tris-HCl (pH 8.0) and 1 mM EDTA) and concentrated by ethanol precipitation, resuspended in $T_{10}E_{0.1}$, and stored at −20 °C. RNA concentrations were quantified by UV absorption at 260 nM (2WJ $\varepsilon_{260} = 8.55 \times 10^5\ M^{-1}\ cm^{-1}$, 4WJ $\varepsilon_{260} = 1.15 \times 10^6\ M^{-1}\ cm^{-1}$).

Incorporation Controls. To control for the level of analogue incorporation at each site, unligated hairpin RNAs were radiolabeled at their 5′-end, cleaved with iodine, and loaded onto sequencing gels as follows. Twenty picomoles of each analogue-incorporated transcript was treated with 50 units of CIP at 37 °C for 1 h. CIP was removed with silica membrane spin columns (Qiagen), and the RNAs were eluted into $T_{10}E_{0.1}$. Each RNA was then 5′-end labeled with 20 units of T4 polynucleotide kinase (PNK) and 150 μCi of [γ-^{32}P]ATP by incubating at 37 °C for 1 h. Labeled RNAs were purified by 8% denaturing PAGE, visualized by autoradiography, excised from the gel, and eluted at 25 °C for 1 h into $T_{10}E_{0.1}$, 250 mM NaCl, and 2% (w/w) SDS, then PCA extracted, ethanol precipitated, and redissolved in a minimal volume of $T_{10}E_{0.1}$. A small aliquot of each solution was scintillation counted, and the remainder was diluted with $T_{10}E_{0.1}$ to provide an equal number of counts per microliter. Each solution was split into two aliquots, treated with iodine ($^1/_{10}$ volume of 100 mM iodine in ethanol) or ethanol alone, denatured at 90 °C in formamide loading buffer (20 mM EDTA in deionized formamide), and run on a 10% denaturing PAGE sequencing gel.

NAIM Ligation Selection. Individual ligation reactions were performed with each of the analogue-incorporated hairpin RNAs and 3′-end-labeled substrates. Hairpin RNAs were first refolded in reaction buffer (50 mM Tris, 10 mM $MgCl_2$, pH = 8.0) by heating to 60 °C for 2 min and cooling to 25 °C over 45 min. Ligation reactions were initiated by adding labeled substrate equilibrated to 25 °C in reaction buffer and mixing. Reaction volumes were typically 20 μL and contained 300 nM hairpin RNA and 20 nM 3′-end-labeled substrate. Unless indicated otherwise, reactions were allowed to proceed for 5 min, which was sufficient time to reach the ligation end point for all construct/substrate pairs. Reactions were quenched with formamide loading buffer and split into two aliquots. Iodine (1.0 μL of 100 mM in ethanol) was added to one aliquot to cleave phosphorothioate linkages, while the other aliquot was treated with ethanol alone to control for nonspecific cleavage. Cleaved and uncleaved samples were denatured at 90 °C and run on 10% denaturing PAGE sequencing gels.

Interference Quantitation. Ligation selection gels and 5′-end-labeled incorporation control gels were dried and exposed to PhosphorImager screens. Sites of interference or enhancement in activity were identified as decreases or increases in band intensity in the ligation selection gel relative to the unligated 5′-end-labeled controls. Because the phosphorothioate substitution can itself lead to changes in activity, a control RNA incorporating the parental 5′-*O*-(1-thio)nucleoside triphosphate was also included. This control was particularly important for the 2WJ hairpin construct where several sites showed significant interference or enhancement arising from the (R_p)-phosphorothioate linkage. For positions A9 and A10 the phosphorothioate effect was so large that quantification of band intensities at these positions in the 2WJ construct was not possible, and interference values for base-modified analogues were not calculated. To quantify sites of interference, line profiles were drawn through ligation selection and control lanes and peak areas calculated. From these peak areas an interference value, κ, was calculated:

$$\kappa = \mathrm{NF}\left(\frac{\mathrm{N\alpha S\ ligation}/\delta\alpha\mathrm{S\ ligation}}{\mathrm{N\alpha S\ 5'control}/\delta\alpha\mathrm{S\ 5'control}}\right)$$

where each member of the fraction is the peak area for a particular site in the ligation or 5′-end-labeled gel, NαS is the parental analogue, and δαS is one of the pK_a perturbed analogues. A normalization factor (NF) is calculated from the ratios to account for uneven loading of the lanes. Interference values calculated in this way normalize both for the extent of analogue incorporation at a particular site and for the effect the phosphorothioate substitution at that site. Interference values between 0.5 and 2.0 are typically viewed as insignificant, while those below 0.5 are expressed as $1/\kappa$ enhancements. Because of the difficulty of accurately quantifying very weak bands interference values above 6.0 are typically treated as equivalent.

Ligation Kinetics and Chase Experiments. Ligation time courses and end points were measured under the same conditions as NAIM ligation reactions except hairpin RNAs transcribed without analogues were used. Chase experiments were conducted after ligation reactions with labeled substrates had reached their end points. For the 11NT substrate chase experiments, a solution containing unlabeled 11NT substrate in reaction buffer was added to 2WJ/7NT or 4WJ/7NT ligations in 3-fold excess relative to the hairpin RNA. For the 4WJ hairpin chase experiments 4WJ RNA was refolded and cooled to 25 °C and then added to 2WJ/7NT or 2WJ/11NT ligations in 1.05-fold excess relative to the hairpin RNA. Reaction aliquots were quenched in formamide loading buffer at the specified time points and run on 20% denaturing PAGE sequencing gels. Gels were exposed to PhosphorImager screens without drying, and the percent ligation was calculated from the substrate and ligation product band intensities.

RESULTS

Construct-Dependent Interference Patterns. We investigated the effect of construct stability and substrate binding affinity on the observed interference patterns by conducting NAIM selections on four construct/substrate pairs under identical reaction conditions (Figure 2). Typical sequencing gels for the ligation selections and incorporation controls were of sufficient quality to calculate interference values for all analogues at adenosine sites 7−43 (Figure 3). The only sites not quantified were A9 and A10 in the 2WJ constructs, due to the large phosphorothioate effects observed at these sites in the minimal construct (Figure 3B,C). Replicate control and selection experiments for each of the analogues yielded a total of 432 average interference values at 19 sites. These data are summarized as a color-coded matrix in Figure 4. As expected, none of the

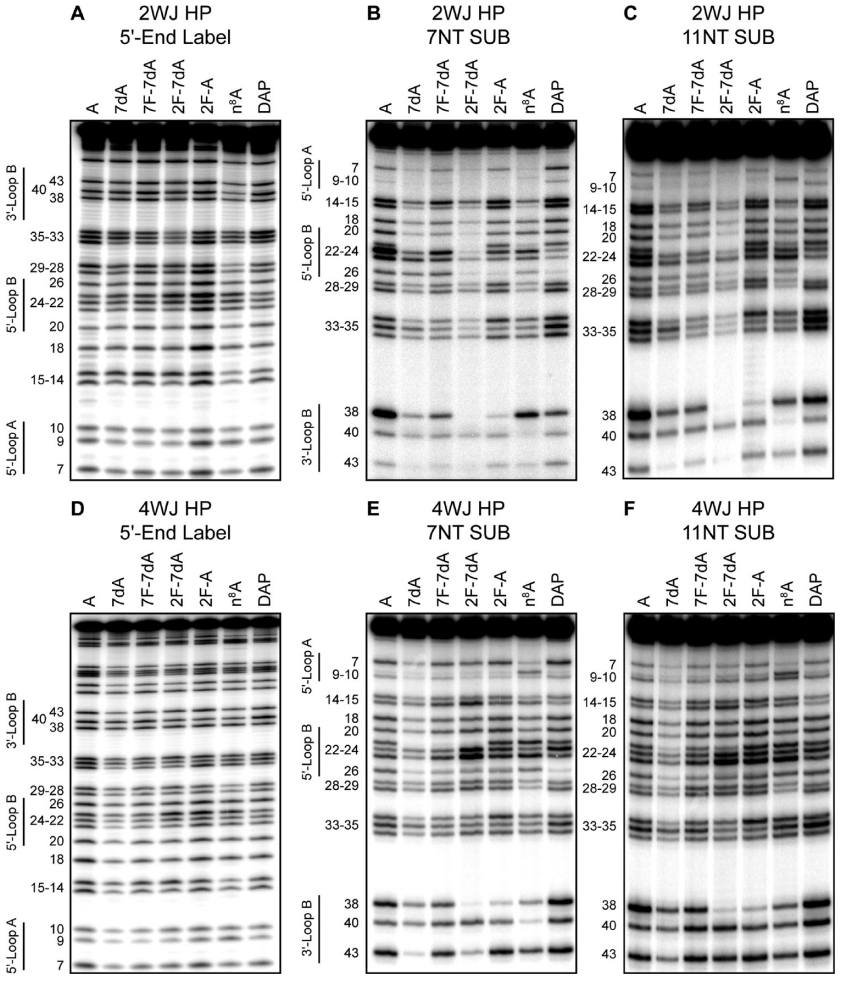

FIGURE 3: Representative interference autoradiograms for the 2WJ construct (A−C) and 4WJ construct (D−F). (A, D) Analogue incorporation controls. (B, E) Ligation selections with 7NT substrate. (C, F) Ligation selections with 11NT substrate. Each lane is labeled with the analogue used, and nucleotide positions are shown to the left with the regions of loops A and B indicated. The order of the bands (top to bottom) for the control and selection sequencing gels is reversed because of the labeling strategy used (see Experimental Procedures).

analogues show any interference in stem−loop IV for any of the construct/substrate pairs. In contrast, the interference pattern for loop B is highly dependent on construct and substrate identity. Every analogue tested showed moderate to large interferences for loop B residues in the 2WJ/7NT selections, while nearly all of these interferences were diminished in more stable construct/substrate pairs (2WJ/11NT and 4WJ/7NT) and absent in the 4WJ/11NT selections.

2-Fluoroadenosine Interference Pattern. Because the focus of this study was to reexplore the role of adenosine ionization in the hairpin reaction, the interference pattern produced by the recently developed 2F-A analogue is of particular interest. This analogue introduces a relatively isosteric fluorine for hydrogen substitution at C2 but possesses an extremely low N1 pK_a, which we previously estimated to be below zero (the first ionization of 2F-A occurs at N7 with a pK_a value of 0.84) (*31*). However, because all purine ring nitrogens and the exocyclic amine are retained in 2F-A, this analogue produces a minimal perturbation to the various hydrogen-bonding interactions of adenosine. Inspection of the 2F-A interference values for each of the hairpin construct/substrate pairs displays a clear transition in the interference pattern as more stable construct/substrate pairs are used in the selection (Figure 4). A38 is the only position that exhibits consistent interference with 2F-A regardless of construct. Even in the 4WJ/11NT selections the interference value at A38 is much larger than the typical upper bound reported ($\kappa > 6$) and can be easily seen in the selection sequencing gel itself (Figure 3F). This pattern of interference suggests that the subtle structural perturbation caused by 2F-A at some sites can be overcome by increasing the stability of the construct used for ligation, while the persistent interference at A38 likely arises from the inability of 2F-A to ionize. Consistent with this interpretation is the interference produced by DAP, which introduces an amino group instead of a fluorine at C2. Inspection of Figure 4 reveals that 2F-A and DAP show similar interference patterns and that their dependence on construct/substrate identity is also similar, with the exception of interference at A38. Strong 2F-A interference persists at A38, while interference produced by DAP at A38 in the 2WJ/7NT pairing is absent in all other construct/substrate pairings. A similar trend is observed for the 2F-7dA analogue, which can be viewed as a low pK_a analogue of 7dA. While the interference caused by 7dA is construct dependent, the 2F-7dA analogue produces strong interferences for all construct/substrate pairs examined.

Interference at A38. The construct-dependent interferences noted above highlight the need to control for subtle structural perturbations when attempting to identify sites of functional ionization. This is particularly true for A38, which exhibits a complex pattern of structural interactions in the reported crystal structures. The residue adopts an unusual syn glycosidic

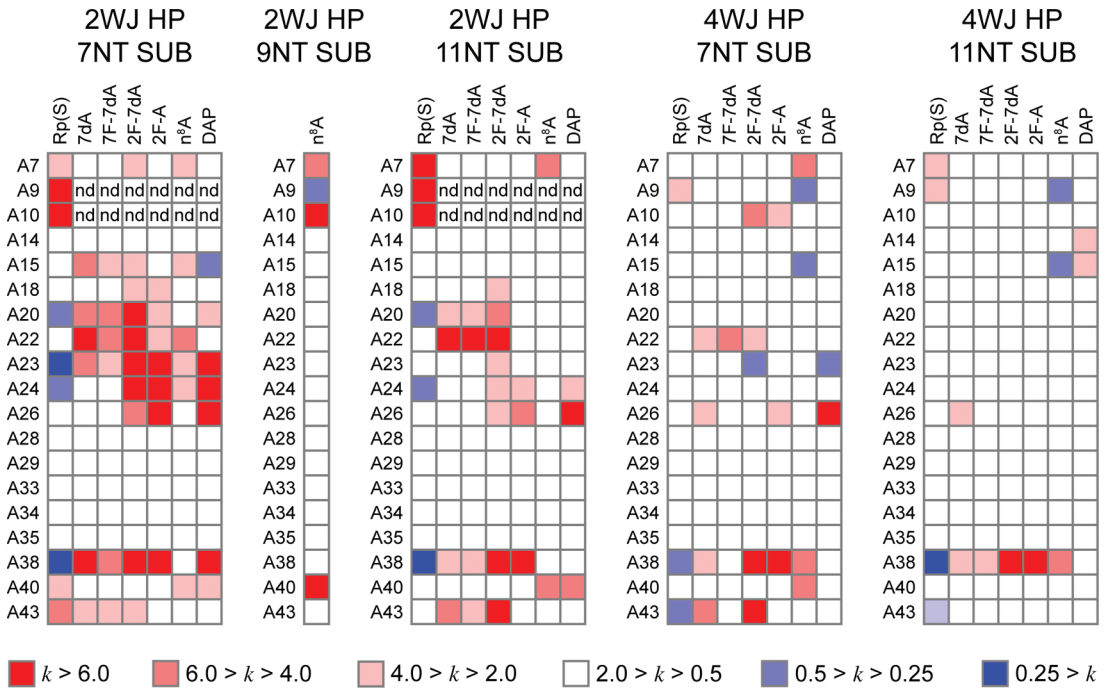

FIGURE 4: Average interference values as a function of analogue (columns) and nucleotide position (rows) for the construct/substrate pairs indicated. The first column of each matrix provides the phosphorothioate effect, which is controlled for in calculating other interference values. Interference values are color coded as indicated from strong interference (deep red) to strong enhancements (deep blue). Sites where large phosphorothioate effects prevented the calculation of interference values are marked "nd". The single column for the n^8A analogue in a 2WJ construct 9NT substrate selection is data taken from our previous study (*21*).

conformation in the docked state, makes hydrogen bonds via its N1, N7, and N6 exocyclic amines, and stacks with the critical G(+1) residue. The new interference patterns reported in this study arise from analogues that make fluorine for hydrogen substitutions at the 2 or 7 position of adenosine or 7-deazaadenosine (Figure 1). To control for structural effects produced by these substitutions, we performed identical NAIM selections with 7dA and DAP. As with other residues in loop B the interference pattern at A38 is dependent on construct/substrate stability for a number of analogues (Figure 4). The exception is interference produced by 2F-A and 2F-7dA, both of which have N1 pK_a values below 1 and exhibit interference values above 6 at A38 for all construct/substrate pairs. Of the remaining analogues 7dA, 7F-7dA, and DAP follow the general trend of decreasing interference with increasing construct/substrate stability. The observation that interference caused by 7-deaza substitutions is mitigated by stabilized constructs is readily explained by a hydrogen bond that involves this nitrogen (*9*, *22*). Consequently, the large construct-independent interference observed for 2F-7dA is likely to originate from the 2-fluoro substitution rather than the 7-deaza substitution. The fact that DAP does not interfere in stabilized constructs indicates the origin of 2F-A and 2F-7dA interference is not a steric effect, suggesting the interference observed with these analogues can be attributed to their low N1 pK_a values.

The construct-dependent interference pattern observed with n^8A at A38 stands in stark contrast to that of the other analogues. The magnitude of n^8A interference at A38 increases in the 4WJ constructs relative to the 2WJ constructs (Figure 4). This pattern of increased interference with increased construct/substrate stability is unique to n^8A interference at A38 and is not observed with n^8A at any other site or with any other analogue at any site. The absence of n^8A interference in the previous study led to the conclusion that A38 was not a site of functional ionization for hairpin catalysis (*21*). The detection of strong interference with n^8A at A38 in stabilized 4WJ constructs is significant because it is the expected interference pattern for functional ionization at this site. Thus, in the most stable construct/substrate pair all analogues with reduced N1 pK_a values show strong interference. An interesting comparison is the construct-dependent interference pattern of 7dA (Figure 4). This pK_a elevated analogue might be expected to produce an enhancement at A38 but instead produces a strong structural interference in the 2WJ/7NT selections that is mitigated in more stable construct/substrate pairs. The analogous interpretation of the construct-dependent n^8A interferences at A38 is that this analogue provides a structural advantage when substituted at A38 in destabilized construct/substrate pairs, while revealing an underlying catalytic deficiency in selections using the most stable construct/substrate pairs.

Equilibration of Reaction Substrates. The interpretation of interference data is highly dependent on whether the steps of substrate binding, docking, and ligation are reversible (see below). Based on the careful analysis of Fedor and colleagues (*2*, *27*), we anticipated our construct/substrate pairs would differ in their ability to reverse these steps and exchange labeled substrates among members of the analogue-incorporated hairpin pool. To test this possibility, we conducted chase experiments under the exact conditions used for NAIM selections (Figure 5). We were particularly interested in whether the reactions were reversible on the time scale of the ligation selections (5 min). When the 2WJ construct was incubated with hot 7NT substrate, an end point of ~30% was reached by 5 min. Addition of an excess of cold 11NT substrate led to a rapid decrease of 2WJ/7NT product on a time scale similar to that of the initial ligation (Figure 5A). The equivalent experiment with the 4WJ construct showed much more rapid formation of the 4WJ/7NT ligation product, with an end point near 55%, but a much slower reversal of this product upon addition of cold 11NT substrate (45% 4WJ/7NT after 5 min quench). These results roughly reproduce what

has been observed previously (*2*), namely, that the cleaved 7NT substrate readily binds and dissociates from the undocked state of both hairpin constructs (*2*) and that the 4WJ construct forms the docked state faster and more stably than the 2WJ construct (*37*). A parallel experiment in which 2WJ/7NT ligation was chased with a slight excess of 4WJ hairpin RNA yielded a comparable result, with the nearly compete conversion of 2WJ/7NT ligated product to 4WJ/7NT ligated product in 5 min (Figure 5B). However, when a 2WJ/11NT ligation was chased with 4WJ hairpin RNA, no conversion to the 4WJ/11NT product was observed. This result confirms the much slower release of the 11NT substrate. Thus in NAIM ligation selections with the 11NT substrate, once substrate binds a member of the analogue-incorporated pool, it does not release before the reaction is quenched.

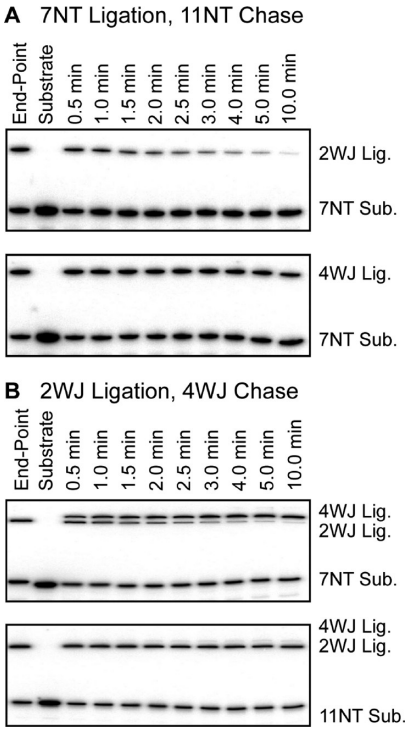

FIGURE 5: Hairpin ligation chase experiments. In each panel the indicated construct/substrate ligation was allowed to reach its end point and then chased with 11NT cold substrate (A) or 4WJ hairpin RNA (B).

Time-Dependent Interference Values. The observation that 7NT substrates rapidly exchange between members of the 2WJ hairpin RNA pool suggested interference values for the 2WJ/7NT ligation might be time dependent. To test this dependence, we repeated the 2WJ/7NT NAIM selections as a function of time for the n^8A and 2F-A analogues (Figure 6A). Significantly, n^8A did show moderate interference at A38 in the 2WJ/7NT selection at our earliest time point (30 s) but had no effect or even slight enhancement at longer times (Figure 6B). This is in contrast to 2F-A, which showed moderate to strong interference at A38 at all ligation time points. The time dependence of n^8A interference is specific to the A38 position. For example, n^8A interference at A23 is consistent at all ligation time points, while the absence of n^8A interference at A14 continues at all ligation time points (Figure 6B). The same consistency is seen for the 2F-A interferences at these sites (Figure 6B). Therefore, in addition to providing the expected interference at A38 in stabilized constructs, n^8A also produces A38 interference at early times of the 2WJ/7NT selections. The equilibration results described above suggest that n^8A interference at A38 is observed before 7NT substrates equilibrate throughout the selection pool via multiple rounds of substrate binding, ligation, cleavage, and release.

DISCUSSION

In the simplest model of hairpin ligation the reaction consists of three steps: (i) binding of substrate via base pairing in helix I,

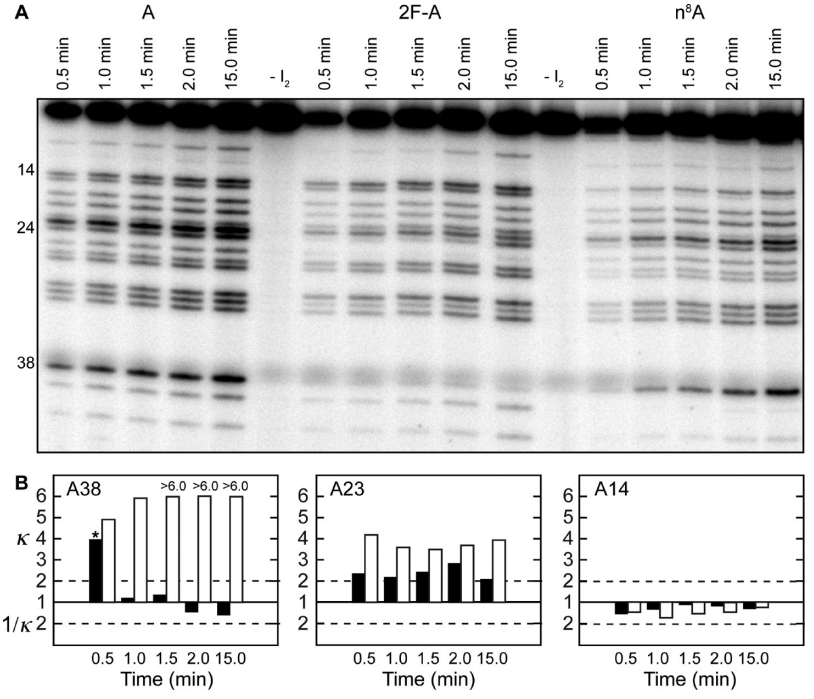

FIGURE 6: Time-dependent NAIM study of the 2WJ/7NT construct/substrate pair. (A) Sequencing gel of ligation selections performed with the indicated analogues as a function of ligation reaction time. (B) Interference values for n^8A (solid bars) and 2F-A (open bars) at the indicated residues as a function of ligation reaction time.

(ii) formation of the condensed docked state mediated by a number of specific interactions between loops A and B, and (iii) the catalyzed attack of the free 5′-OH at G(+1) on the cyclic 2′,3′-phosphate at the N(−1) position (*8*) (Figure 7). Hairpin-catalyzed cleavage is simply the reverse of these steps, resulting in dissociated substrate and a cleaved hairpin RNA capable of another ligation reaction. Single molecule FRET studies have shown that the sequence of at least these steps can be obligate, indicating that bound substrates must dock before ligation and cleaved substrates must undock before release in certain constructs (*38*). Furthermore, the energetics of these steps are not easily separated (*36*), as indicated by the fact that more stably docked constructs also exhibit an internal equilibrium significantly shifted toward ligation (*2*). A challenge in interpreting nucleotide modification experiments is dissecting the contribution made by chemical and structural steps along the reaction pathway. This is particularly true for the hairpin ribozyme, where the rate-limiting step has been shown to be construct dependent (*38*) and where some of the most detrimental base modifications are now known to be structural in origin (*26*).

The introduction of nucleobase modifications further complicates this picture since substitution at one site with a given analogue may introduce a defect in docking, while substitution at another site with the same analogue may introduce a defect in ligation chemistry. In the context of NAIM experiments, this situation might result in strong interference with a given analogue at two different sites arising from completely different origins. In an attempt to deconvolute these effects in the hairpin ligation reaction, we conducted a NAIM analysis with a structurally similar series of analogues using construct/substrate pairs expected to exhibit distinctly different kinetics in the steps prior to chemistry. The ligation chase experiments indicate that this is indeed the case under our NAIM selection conditions and that the interference patterns observed represent a progression between two extremes. In the context of the 2WJ/7NT reaction, ligation reactions reach full equilibrium among the analogue-incorporated pool. This means any given substrate will complete a full reaction cycle (bind, dock, ligate, cleave, undock, and release) from several members of the analogue-incorporated pool before the reaction is quenched. In this extreme, members that stabilize the ligated docked state accumulate in the active fraction, and members deficient in either docking or chemistry are underrepresented. The ability of labeled substrates to exchange between members of the hairpin ribozyme pool through cleavage and release accentuates deficiencies in docking, since the ability of cleaved substrates to release is dependent on the formation of the undocked state for some constructs. Ligation selections carried out with the 4WJ/11NT substrate represent the opposite extreme. In these reactions labeled substrates bind members of the analogue-incorporated pool and are not released during the time course of the selection, whether ligated or not. Here the active fraction is determined primarily by the internal ligation/cleavage equilibrium. The 2WJ/11NT and 4WJ/7NT reaction pairs lie between these extremes. In the 2WJ/11NT pair, the docked state is destabilized relative to the 4WJ/11NT pair, but cleaved substrate is not released to equilibrate with other members of the selection pool. In the 4WJ/7NT pair, the docked state is stabilized relative to the 2WJ/7NT pair, but the undocked fraction will release cleaved substrate to equilibrate with the selection pool.

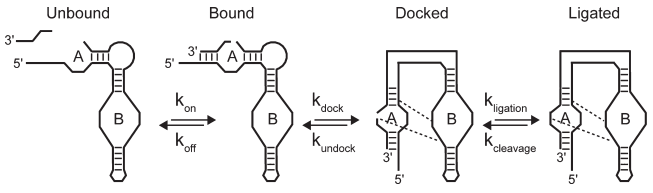

FIGURE 7: Minimum reaction sequence for hairpin ligation, consisting of substrate binding, the formation of a docked state requiring specific interactions between residues in loops A and B (dashed lines), and ligation between G(+1) and N(−1). All steps are reversible, with the equilibrium dependent on the energetics of substrate binding, the stability of the docked state, and the ribozyme-catalyzed equilibrium between ligation and cleavage.

The construct dependence of the observed interferences can be used to differentiate those modifications that primarily affect docking stability from those that affect chemistry. For example, all of the adenosine residues in the A-rich loop from A20 to A26 show strong interference with one or more analogues in the context of the 2WJ/7NT reaction pair. These interferences decrease systematically as more stable construct/substrate pairs are used in the selection. Tertiary interactions within the hairpin crystal structures readily explain many of these interferences. For example, the strong interference of 7-deaza substitutions at A22 likely arises from this base's involvement in the positioning of U42 at the interface of loop B and helix II in the docked state (Figure 8C). The unusual turn between U41 and U42 that allows U42 to bridge loop B and helix II relies on hydrogen bonds to the exocyclic amine and N7 nitrogen of A22. Removal of the N7 nitrogen at A22 disrupts this interaction, leading to a destabilized

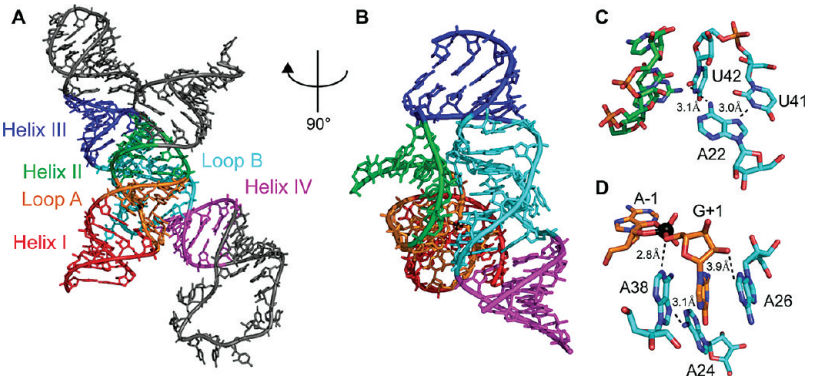

FIGURE 8: (A) Crystal structure of a 4WJ construct with a vanadate transition state mimic (*9*), color coded by helices I−IV and loops A and B. (B) Rotated view emphasizing the docking interface between loop B and helix II/loop A. (C) Involvement of A22 in orienting U42 at the loop B/helix II interface. (D) Adenosine residues in vicinity of G(+1) and the vanadate transition state mimic (black ball).

docked state and interference in less stable constructs. Many of the construct-dependent interferences can be explained in a similar manner by observed or anticipated contacts in the available crystal structures.

The primary goal of this study was to reinvestigate functional adenosine ionization with a new series of pK_a perturbed analogues. The extreme sensitivity of interference values to construct/substrate stability suggests that interferences arising from catalytic steps are best identified in stabilized construct/substrate pairs. As noted above, A38 is the only site that shows strong interferences that persist in the most stable constructs (Figure 4). The pattern of interference at A38 is consistent with N1 ionization, with all low pK_a analogues showing interference at this site in the 4WJ/11NT reaction pair. However, as in our earlier study we failed to observe n^8A interference in reactions with 2WJ constructs. One possible explanation for this result is that n^8A substitution at A38 simultaneously slows the rate of ligation but increases the stability of the docked state. In this scenario a defect in catalysis would be compensated for by an increased lifetime in the active conformation. This advantage would be eliminated in constructs where the stability of the docked state equalizes the smaller stability differences introduced by analogue substitution. The concept that ligation with n^8A at A38 is kinetically slower but more favored at equilibrium in the 2WJ construct is supported by the time-dependent interference pattern seen with this analogue (Figure 6B).

Taken together, the construct and time dependence of n^8A interference at A38 suggests functional ionization at this site was missed in our previous study because this analogue stabilizes the docked state, masking its effect on catalysis in the least stable hairpin constructs. Although our NAIM data do not directly reveal the origin of this docking advantage, they do suggest the effect is unique to A38, since it is the only site where n^8A substitution produces a distinctive pattern of larger interferences (or smaller enhancements) in more stabilized constructs. Interestingly, A38 is also the only adenosine nucleotide that adopts a syn glycoside conformation in any of the reported crystal structures (*9*, *10*, *22*). This rare nucleoside conformation is not observed at A38 in the isolated loop B NMR structure (*24*), suggesting an anti to syn transition is part of the large structural reorganization that occurs between the extended and docked states. The fact that n^8A exhibits a decreased barrier of rotation to the syn conformation (*39*) provides a reasonable explanation for its selective advantage in destabilized constructs. Indeed, substrate helix docking can be rate limiting in minimal hairpin constructs under some conditions, with the undocked fraction existing in multiple states, one or more of which may involve an anti to syn transition at A38 along the folding pathway. The requirement of a syn conformation at A38 to form the fully docked state could also explain the interference produced by 7dA in destabilized constructs, since the observed hydrogen bond between the N7 of A38 and the N6 amine of A24 is also absent from the undocked NMR structure and acts to stabilize the syn conformation (Figure 8D).

Overall, the interference data obtained in this study argue for functional ionization at A38, consistent with a wealth of structural data and a number of site-specific modification experiments. A38 was the only site that showed persistent and strong interference with low pK_a analogues across a variety of construct/substrate pairs. As in our previous study we failed to observe interference with n^8A at A38 in destabilized constructs. However, by employing stably docked constructs or by quenching destabilized constructs at early times, n^8A interference at A38 was observed. These results suggest that n^8A is deficient in the chemical step of ligation but compensates for slow chemistry by stabilizing the docked state. The origin of this docking advantage may be the increased propensity of n^8A to form the required syn glycoside conformation. In contrast, the low pK_a fluoroadenosine analogues produced strong and construct-independent interference at A38, suggesting these analogues are better suited to identify sites of functional ionization in systems where structural rearrangements are closely coupled to catalytic steps.

REFERENCES

1. Fedor, M. J. (2009) Comparative enzymology and structural biology of RNA self-cleavage. *Annu. Rev. Biophys. Biomol. Struct. 38*, 271–299.
2. Fedor, M. J. (1999) Tertiary structure stabilization promotes hairpin ribozyme ligation. *Biochemistry 38*, 11040–11050.
3. Buzayan, J. M., Gerlach, W. L., Bruening, G., Keese, P., and Gould, A. R. (1986) Nucleotide sequence of satellite tobacco ringspot virus-RNA and its relationship to multimeric forms. *Virology 151*, 186–199.
4. Spitale, R. C., Volpini, R., Heller, M. G., Krucinska, J., Cristalli, G., and Wedekind, J. E. (2009) Identification of an imino group indispensable for cleavage by a small ribozyme. *J. Am. Chem. Soc. 131*, 6093–6095.
5. Spitale, R. C., Volpini, R., Mungillo, M. V., Krucinska, J., Cristalli, G., and Wedekind, J. E. (2009) Single-atom imino substitutions at A9 and A10 reveal distinct effects on the fold and function of the hairpin ribozyme catalytic core. *Biochemistry 48*, 7777–7779.
6. Macelrevey, C., Salter, J. D., Krucinska, J., and Wedekind, J. E. (2008) Structural effects of nucleobase variations at key active site residue Ade38 in the hairpin ribozyme. *RNA 14*, 1600–1616.
7. Salter, J., Krucinska, J., Alam, S., Grum-Tokars, V., and Wedekind, J. E. (2006) Water in the active site of an all-RNA hairpin ribozyme and effects of Gua8 base variants on the geometry of phosphoryl transfer. *Biochemistry 45*, 686–700.
8. Wilson, T. J., Nahas, M., Araki, L., Harusawa, S., Ha, T., and Lilley, D. M. J. (2007) RNA folding and the origins of catalytic activity in the hairpin ribozyme. *Blood Cells, Mol. Dis. 38*, 8–14.
9. Rupert, P. B., Massey, A. P., Sigurdsson, S. T., and Ferre-D'Amare, A. R. (2002) Transition state stabilization by a catalytic RNA. *Science 298*, 1421–1424.
10. Torelli, A. T., Krucinska, J., and Wedekind, J. E. (2007) A comparison of vanadate to a 2′-5′ linkage at the active site of a small ribozyme suggests a role for water in transition-state stabilization. *RNA 13*, 1052–1070.
11. Tan, E., Wilson, T. J., Nahas, M. K., Clegg, R. M., Lilley, D. M. J., and Ha, T. (2003) A four-way junction accelerates hairpin ribozyme folding via a discrete intermediate. *Proc. Natl. Acad. Sci. U.S.A. 100*, 9308–9313.
12. Walter, N. G., Burke, J. M., and Millar, D. P. (1999) Stability of hairpin ribozyme tertiary structure is governed by the interdomain junction. *Nat. Struct. Biol. 6*, 544–549.
13. Nesbitt, S., Hegg, L. A., and Fedor, M. J. (1997) An unusual pH-independent and metal-ion-independent mechanism for hairpin ribozyme catalysis. *Chem. Biol. 4*, 619–630.
14. Kuzmin, Y. I., Da Costa, C. P., and Fedor, M. J. (2004) Role of an active site guanine in hairpin ribozyme catalysis probed by exogenous nucleobase rescue. *J. Mol. Biol. 340*, 233–251.
15. Nesbitt, S. M., Erlacher, H. A., and Fedor, M. J. (1999) The internal equilibrium of the hairpin ribozyme: Temperature, ion and pH effects. *J. Mol. Biol. 286*, 1009–1024.
16. Fedor, M. J. (2000) Structure and function of the hairpin ribozyme. *J. Mol. Biol. 297*, 269–291.
17. Suydam, I. T., and Strobel, S. A. (2009) Nucleotide analog interference mapping. *Methods Enzymol. 468*, 3–30.
18. Waldsich, C. (2008) Dissecting RNA folding by nucleotide analog interference mapping (NAIM). *Nat. Protoc. 3*, 811–823.
19. Cochrane, J. C., and Strobel, S. A. (2004) Current Protocols in Nucleic Acid Chemistry, Vol. *2*, Wiley, New York.
20. Ryder, S. P., and Strobel, S. A. (1999) Nucleotide analog interference mapping of the hairpin ribozyme: Implications for secondary and tertiary structure formation. *J. Mol. Biol. 291*, 295–311.
21. Ryder, S. P., Oyelere, A. K., Padilla, J. L., Klostermeier, D., Millar, D. P., and Strobel, S. A. (2001) Investigation of adenosine base

ionization in the hairpin ribozyme by nucleotide analog interference mapping. *RNA 7*, 1454–1463.
22. Rupert, P. B., and Ferre-D'Amare, A. R. (2001) Crystal structure of a hairpin ribozyme-inhibitor complex with implications for catalysis. *Nature 410*, 780–786.
23. Cai, Z. P., and Tinoco, I. (1996) Solution structure of loop A from the hairpin ribozyme from tobacco ringspot virus satellite. *Biochemistry 35*, 6026–6036.
24. Butcher, S. E., Allain, F. H. T., and Feigon, J. (1999) Solution structure of the loop B domain from the hairpin ribozyme. *Nat. Struct. Biol. 6*, 212–216.
25. Ryder, S. P., and Strobel, S. A. (2002) Comparative analysis of hairpin ribozyme structures and interference data. *Nucleic Acids Res. 30*, 1287–1291.
26. Ferre-D'Amare, A. R. (2004) The hairpin ribozyme. *Biopolymers 73*, 71–78.
27. Kuzmin, Y. I., Da Costa, C. P., Cottrell, J. W., and Fedor, M. J. (2005) Role of an active site adenine in hairpin ribozyme catalysis. *J. Mol. Biol. 349*, 989–1010.
28. Gaur, S., Heckman, J. E., and Burke, J. M. (2008) Mutational inhibition of ligation in the hairpin ribozyme: Substitutions of conserved nucleobases A9 and A10 destabilize tertiary structure and selectively promote cleavage. *RNA 14*, 55–65.
29. Bevilacqua, P. C. (2003) Mechanistic considerations for general acid-base catalysis by RNA: Revisiting the mechanism of the hairpin ribozyme. *Biochemistry 42*, 2259–2265.
30. Guo, M., Spitale, R. C., Volpini, R., Krucinska, J., Cristalli, G., Carey, P. R., and Wedekind, J. E. (2009) Direct Raman measurement of an elevated base pK(a) in the active site of a small ribozyme in a precatalytic conformation. *J. Am. Chem. Soc. 131*, 12908–12909.
31. Suydam, I. T., and Strobel, S. A. (2008) Fluorine substituted adenosines as probes of nucleobase protonation in functional RNAs. *J. Am. Chem. Soc. 130*, 13639–13648.
32. Jones, F. D., and Strobel, S. A. (2003) Ionization of a critical adenosine residue in the *Neurospora* Varkud satellite ribozyme active site. *Biochemistry 42*, 4265–4276.
33. Smith, M. D., and Collins, R. A. (2007) Evidence for proton transfer in the rate-limiting step of a fast-cleaving Varkud satellite ribozyme. *Proc. Natl. Acad. Sci. U.S.A. 104*, 5818–5823.
34. Zhao, Z. Y., McLeod, A., Harusawa, S., Araki, L., Yamaguchi, M., Kurihara, T., and Lilley, D. M. J. (2005) Nucleobase participation in ribozyme catalysis. *J. Am. Chem. Soc. 127*, 5026–5027.
35. Lafontaine, D. A., Wilson, T. J., Zhao, Z. Y., and Lilley, D. M. J. (2002) Functional group requirements in the probable active site of the VS ribozyme. *J. Mol. Biol. 323*, 23–34.
36. Cottrell, J. W., Kuzmin, Y. I., and Fedor, M. J. (2007) Functional analysis of hairpin ribozyme active site architecture. *J. Biol. Chem. 282*, 13498–13507.
37. Nahas, M. K., Wilson, T. J., Hohng, S. C., Jarvie, K., Lilley, D. M. J., and Ha, T. (2004) Observation of internal cleavage and ligation reactions of a ribozyme. *Nat. Struct. Mol. Biol. 11*, 1107–1113.
38. Zhuang, X. W., Kim, H., Pereira, M. J. B., Babcock, H. P., Walter, N. G., and Chu, S. (2002) Correlating structural dynamics and function in single ribozyme molecules. *Science 296*, 1473–1476.
39. Singh, P., and Hodgson, D. J. (1977) 8-Azaadenosine—Crystal structure of its monohydrate and conformational analysis for rotation around glycosyl bond. *J. Am. Chem. Soc. 99*, 4807–4815.
40. Saenger, W. (1984) Principles of nucleic acid structure, Springer-Verlag, New York.